Computers and Mathematics with Applications 73 (2017) 2603–2617

Contents lists available at ScienceDirect

Computers and Mathematics with Applications

journal homepage: www.elsevier.com/locate/camwa

Galerkin finite element method for cancer invasion mathematical model

Sashikumaar Ganesan [a], Shangerganesh Lingeshwaran [a,b,*]

[a] Department of Computational and Data Sciences, Indian Institute of Science, Bangalore, 560 012, India
[b] Department of Humanities and Sciences, National Institute of Technology, Goa, 403 401, India

ARTICLE INFO

Article history:
Received 20 May 2016
Received in revised form 3 April 2017
Accepted 9 April 2017
Available online 5 May 2017

Keywords:
Cancer invasion
PDE cancer model
Haptotaxis effect
Finite element simulations

ABSTRACT

A finite element scheme for the solution of a cancer invasion model is proposed. The cancer dynamics model consists of three coupled partial differential equations which describe the evolution of cancer cell density, extra cellular matrix and the matrix degrading enzymes. The model incorporates proliferation and haptotaxis effect of cancer cells, their interaction with extracellular matrix, the production of matrix degrading enzymes and consequent degradation of the extracellular matrix. The coupled partial differential equations are discretized in space with the standard Galerkin finite elements and in time with the Crank–Nicolson method. Moreover, the nonlinear terms in the coupled equations are treated semi-implicitly in the finite element scheme. The numerical scheme is validated with numerical results taken from the literature. In addition to the mesh convergence study, the effects of haptotactic rate, proliferation rate and remodelling rate of matrix components of the considered mathematical model are investigated.

1. Introduction

All living organisms are composed of a collection of cells, which grow and divide in a controlled manner with a certain order for the proper functioning of the organism. Sometimes cells start to grow without considering the normal balance between the growth and the death. Also, there is a cell migration between neighbouring tissues. Cells with these hostile behaviours are called cancer cells or tumour. In order to understand this disease better and to analyse the response of cancer cells to treatments, an increasing number of mathematical models have been applied, see, for example [1–9] and the references therein. Many researchers are actively involved in the cancer modelling over the past three decades. Not only the clinical applications, but also the mathematical and numerical challenges associated with the solution of the coupled nonlinear cancer growth models have attracted many applied mathematicians. We briefly recall the dynamics of the tumour growth that involves proliferation, invasion of the host tissue and spread to other parts of the body. Subsequently, various mathematical models proposed in the literature for the tumour growth are reviewed in this section.

Tumour growth is a process that involves a sequence of complex events. *In vivo* cancer evolution starts with seeding and growth of primary tumours in particular location or in organ of the body. In this initial avascular stage, the tumour size is restricted up to a few millimetres of diameter. Cancer cells produce degrading enzymes (e.g. matrix metalloproteinases) that help to invade the host tissue (e.g. extra cellular matrix). Further, the tumour becomes malignant when the primary tumour locally invades the host tissue, and spreads to over distant sites of the body to establish secondary tumours. The process of spreading and formation of secondary tumours are called metastasis [10,11].

* Corresponding author at: Department of Humanities and Sciences, National Institute of Technology, Goa, 403 401, India.
E-mail addresses: sashi@cds.iisc.ac.in (S. Ganesan), shangerganesh@nitgoa.ac.in (S. Lingeshwaran).

http://dx.doi.org/10.1016/j.camwa.2017.04.006
0898-1221/

Moreover, a blood supply is necessary for the transition of avascular phase to the vascular phase. Cancer cells induce chemical signals that stimulate angiogenesis, i.e. the formation of new blood vessels or proliferation of capillaries, to obtain blood supply [4,12] and it is called tumour angiogenesis. Further, the growth of tumour cell is only possible when the capillaries penetrate into the tumour. Experimental and theoretical observations confirm that the capillary proliferation is stimulated by the tumour angiogenesis factor released by the solid tumours [4,5,13]. This process occurs in vascularized phase.

In order to detect the progression of tumour in a relatively less time without a huge cost of laboratory experiments, a number of mathematical models have been proposed in the literature. These models can be classified (see, [10]) into three categories: (i) ordinary differential equation (ODE) models, (ii) partial differential equation (PDE) models, and (iii) discrete models. ODE models describe the evolution of the cancer cells population growth rather than the growth of an individual cancer cell [14,15]. Since the tumour growth decelerates as it grows bigger, dynamic growth models have also been used in the ODE models, see [16,17] and the references therein for an overview of ODE models.

Even though the ODE models have successfully been used to compute the time evolution of the cancer cell population, the consideration of spatially independent population growth is the most apparent shortcoming of the ODE models. In addition to the tumour invasion, the spread of primary cancer cells to other parts of the body to establish secondary tumours (metastasis) is the main cause of mortality among cancer patients. Therefore, the spatial dependency of the tumour invasion and the metastasis are also need to be considered in the mathematical models to realistically simulate the clinical observations. It necessitates the PDE models in the field of cancer biology.

Originally, Gatenby and Gawlinski [7] proposed a spatio-temporal cancer invasion model that contains three coupled PDEs to describe the development of the tumour, the interaction of tumour with the normal cells and the production of H^+ ions by tumour, respectively. The authors compared the numerical results with the existing experimental data and clinical observations. Recently, the same model has been generalized to incorporate the competitive growth of cells and the acid mediated cancer cell death [18]. Also we refer to the papers [19–22] for more details on acid mediated cancer invasion models. In general, cancer cells produce matrix degrading enzymes (MDE) that degrade the extracellular matrix (ECM). This micro environment process has been modelled in [23] together with the spatio-temporal cancer invasion model proposed in [7].

Haptotaxis is the movement of cancer cells towards the gradient direction of the ECM density. This effect plays a key role in the cancer cell invasion process. Anderson et al. [24] proposed a PDE model with haptotaxis effect which describes the growth of the cancer density, the ECM density and the MDE concentration. However, the cancer growth rate has not been considered in [24]. Later, the haptotaxis PDE model proposed in [24] has been extended in [25] to incorporate the competitive growth (proliferation) of the cancer cells and the ECM density. Instead of considering a single MDE concentration equation, Chaplain and Lolas [6] have proposed a model with urokinase-type plasminogen activator (uPA) system. This model describes the interaction of cancer cells, ECM, uPA, plasminogen activators and plasmin. Alternative to the uPA system, Deakin and Chaplain [26] proposed a PDE model to study the role of membrane-bound matrix metalloproteinases.

The cancer cell invasion is also achieved through the loss of cell–cell adhesion and enhanced cell–matrix adhesion. This process has been modelled by replacing the local haptotaxis flux term proposed in [25] with a non-local (spatially) flux term in [27]. This model has further been studied in [28] to demonstrate that the model is capable of supporting both noninvasive and invasive tumour growth according to the relative strength of cell–cell to cell–matrix adhesion. Very recently, Domschke et al. [29] extended the model proposed in [27] for multiple cancer cell populations.

More studies on the above mentioned models with applications to glioma growth [30], breast tumours [31–33] as well as to metastasis tumours [34,35] have been presented in the literature. Mathematical analysis such as linear stability analysis, pattern formation of solutions, existence of solutions, have also been performed by several authors, see for example, [4,36–40]. Moreover, mathematical models that describe the tumour angiogenesis [2,4,5,41–44,71] and deal the vascularized tumours [4,45,46] and tumour growth on basis of the continuum theory of mixtures [47] have also been developed and studied in the literature. In addition to the continuum models, hybrid continuum-discrete mathematical models have also been proposed [1,48]. For more detailed reviews on the modelling of tumour invasion, we refer to [3,10,49,50,9].

In this paper, we proposed a finite element scheme for the avascular cancer invasion model. The considered PDE model is one of the variants of the models proposed in [24,6,32,40]. This model is capable of describing the invasion and metastasis behaviours of the tumour in a detailed manner using cancer cell migration, cancer cell proliferation, ECM degradation and ECM remodelling. Nevertheless, the extension of the proposed numerical scheme for the advanced cancer invasion model is straightforward. Numerical schemes based on the method of lines have been widely used for simulations of the cancer invasion process, see for example, [29,27]. In addition, finite difference method [51], finite volume method [52,53], spectral element method [71] have also been proposed in the literature for the related cancer invasion model.

Even though finite element schemes such as positivity preserving finite element method [54], discontinuous Galerkin element method [55], level set/adaptive finite element method [56–58,8,59], a hybrid finite volume/finite element [60] have been proposed in the literature for chemotaxis and angiogenesis models. It is the purpose of this paper to develop and implement an accurate and efficient finite element scheme for the PDE model with avascular cancer invasion and metastasis. Though a standard Galerkin finite element scheme is used in this paper, the application of stabilization method such as streamline upwind/Petrov Galerkin (SUPG), local projection stabilization (LPS) [61], extension to higher dimensions and other advanced models is straightforward in the used in-house code [62]. Thus, the main focus of this paper is to develop

and validate a finite element scheme for the considered cancer model. The optimal order of convergence for the proposed scheme is shown for problems with known analytical solutions. Further, the scheme is validated by comparing with the existing numerical results in the literature. Simulations of cancer cell density growth as well as its interaction with ECM and the degradation of ECM by MDE are performed.

Moreover, the tumour evolution depends on several parameters, and the influence of each parameter needs to be understood for an effective cancer treatment. Therefore, in addition to the implementation and validation of the proposed finite element scheme, our goal is also to understand the effects of haptotactic rate, proliferation rate and remodelling rate of ECM on cancer invasion for different parameters. Thus, different numerical experiments are performed to make a parametric study for the parameters used in the model.

The paper is organized as follows. In Section 2, cancer invasion model consisting of cancer density equation, ECM density equation and MDE concentration equation is presented. Further, the dimensionless form of the model equations is presented in this section. Finite element variational formulation, spatial–temporal discretizations, solution procedure for the nonlinear system are presented in Section 3. The mesh convergence and validation of the proposed numerical scheme are presented in Section 4 together with the effects of haptotactic rate, cancer cell proliferation rate and ECM remodelling. Finally, we summarize the observations of this study and conclude the paper with an outlook.

2. Mathematical model

We consider a two-dimensional partial differential equation model for cancer invasion and growth. The model consists of three unknown variables namely the cancer cell density, ECM density and MDE concentration and denoted by u, v, and w respectively. A brief description of the biological process and its corresponding models are given here. Let $\Omega = [0, 1]\times[0, 1]$ be the computational domain and $\partial\Omega$ be its boundary. Further, the derivation of the dimensionless form of the model equations is provided here for the completeness.

We have considered the cancer invasion mathematical model proposed in [24], and modified in [32] to incorporate cancer cell proliferation and added the effects of ECM remodelling in [40]. Further, we have extended the model to two dimensions and hence, the corresponding model is given by

$$\left.\begin{aligned} \frac{\partial u}{\partial t} - D_u\Delta u + \nabla\cdot(\chi_0 u\nabla v) &= \mu u\left(1-\frac{u}{U}-\frac{v}{V}\right) && \text{in } \Omega\times(0,I),\\ \frac{\partial v}{\partial t} &= -kvw+\rho_v v\left(1-\frac{u}{U}-\frac{v}{V}\right) && \text{in } \Omega\times(0,I),\\ \frac{\partial w}{\partial t} - D_w\Delta w &= \zeta u\left(1-\frac{w}{W}\right)-\gamma w && \text{in } \Omega\times(0,I), \end{aligned}\right\} \tag{2.1}$$

where diffusion coefficients D_u and D_w of u and w respectively are assumed as constants and $t \in [0, I]$ is the time. Here, χ_0 is the haptotactic rate, and μ is a proliferation rate of cancer cells. Further, k and ρ_v are degradation and remodelling rate of ECM respectively. Moreover, the growth and decay rate of MDE are given by ζ and γ respectively. Further, χ_0, μ, k, ρ, ζ and γ are positive constants.

2.1. Dimensionless form

Let $L = 0.1$ cm and $\tau = \frac{L^2}{D}$, (where $D \simeq 10^{-6}$ cm^2 s^{-1} [25]) be the characteristic length and time scales, respectively and we define the dimensionless variables as

$$\tilde{u} = \frac{u}{U}, \qquad \tilde{v} = \frac{v}{V}, \qquad \tilde{w} = \frac{w}{W}, \qquad \tilde{x} = \frac{x}{L}, \qquad \tilde{t} = \frac{t}{\tau}.$$

Further, the values of reference densities u, and v are assumed 6.7×10^7 cell/cm^3, 10^{-10} M respectively as in [1,27] and the reference MDE concentration is unspecified due to difficulties in obtaining suitable experimental values, see [1,27]. Applying these dimensionless variables to system (2.1), and omitting the tilde afterwards, the dimensionless form of the model equations (2.1) in $\Omega \times (0, I)$ becomes:

$$\left.\begin{aligned} \frac{\partial u}{\partial t} - d_1\Delta u + \nabla\cdot(\chi u\nabla v) - \lambda u(1-u-v) &= 0,\\ \frac{\partial v}{\partial t} + \eta vw - \rho v(1-u-v) &= 0,\\ \frac{\partial w}{\partial t} - d_2\Delta w - \alpha u(1-w) + \beta w &= 0. \end{aligned}\right\} \tag{2.2}$$

Here,

$$d_1 = \frac{\tau D_u}{L^2}, \qquad d_2 = \frac{\tau D_w}{L^2}, \qquad \lambda = \tau\mu, \qquad \chi = \frac{\chi_0 V\tau}{L^2}, \qquad \eta = \tau kW,$$

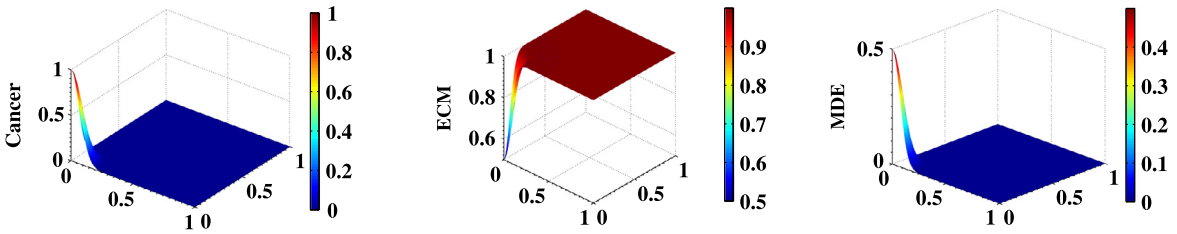

Fig. 1. Initial conditions of the cancer cell density, ECM density and MDE concentration.

Table 1
Parameter choice of the model.

Parameters	Dimensional range	Non-dimensional range	References
Cancer diffusion coefficient (d_1)	10^{-9}–10^{-11} cm^2 s^{-1}	10^{-3}–10^{-5}	[63,5,6,64,65]
MDE diffusion coefficient (d_2)	10^{-9}–10^{-11} cm^2 s^{-1}	10^{-3}–10^{-5}	[63,5,6,64,65]
Cancer proliferation rate (λ)	0.02–0.72 h^{-1}	0.05–2	[25,45,64,66]
MDE decay rate (β)	–	0.1–1	[67,25,6,40]
Haptotaxis coefficient (χ)	–	0.001–1	[25,6]
ECM degradation rate (η)	–	1–20	[25,6,40]
ECM remodelling rate (ρ)	–	0.15–10	[25,6,40]
MDE growth rate (α)	–	0.05–1	[25,6,40]

$$\alpha = \tau\zeta\frac{U}{W}, \qquad \beta = \tau\gamma, \qquad \rho = \rho_v\tau$$

are dimensionless quantities and see Table 1.

2.2. Initial and boundary conditions

It is assumed that both the interactions of cancer cells with the ECM and degradation of the ECM by MDE takes place in an isolated system. Hence, the zero-flux type boundary conditions for the unknown space–time functions u and w are imposed as in [27], that is,

$$(-d_1\nabla u + \chi u\nabla v)\cdot n = 0, \qquad (-d_2\nabla w)\cdot n = 0, \qquad \text{on } \partial\Omega\times[0,I]$$

where n is the outward normal vector on $\partial\Omega$. Further, the following initial conditions

$$\begin{aligned} u(x,0) &= \begin{cases} \exp\left(\dfrac{-r^2}{\epsilon}\right), & r\in[0,0.25] \\ 0, & r\in(0.25,1]. \end{cases} \\ v(x,0) &= 1-0.5u(x,0), \\ w(x,0) &= 0.5u(x,0), \quad \text{in } \Omega \end{aligned} \tag{2.3}$$

are considered for the given system (2.2) with $\epsilon = 0.01$ and presented in Fig. 1.

3. Finite element scheme

The mathematical model considered in the previous section is a highly nonlinear coupled system of partial differential equations. Thus solving the system (2.2) analytically is a tough task. Therefore, a finite element scheme is presented in this section. We first derive variational forms of the cancer cells density equation, ECM density equation and the MDE concentration equation. Further, temporal discretizations of the model equations are presented. In addition an iteration of fixed point type is described to handle the nonlinear terms in the cancer parabolic system. Finally, we define the finite element ansatz functions for each unknown and provide the spatial discretization of the system (2.2).

3.1. Variational formulation

Let $L^2(\Omega)$ and $H^1(\Omega)$ be the usual Lebesgue and Hilbert spaces, respectively, and $(\cdot,\cdot)$ denotes the inner product in $L^2(\Omega)$. Let $L^2(0,I,H^1(\Omega))$ be the solution space for the cancer cell density, ECM density and MDE concentration.

We now derive the variational form of the cancer invasion system (2.2) by multiplying each equation in the system by a test function $\phi\in H^1(\Omega)$, and integrate over Ω. After applying integration by parts to the higher order derivative terms and imposing the no flux boundary condition, the variational form of the system reads:

For given $u_0, v_0, w_0 \in L^2(\Omega)$ find $u, v, w \in L^2(0, I, H^1(\Omega))$ with $u', v', w' \in L^2(0, I, H^{-1}(\Omega))$ such that

$$\left.\begin{aligned} \left(\frac{\partial u}{\partial t}, \phi\right) + a_u(u; u; v, \phi) &= 0, \\ \left(\frac{\partial v}{\partial t}, \phi\right) + a_v(v; v; u; w, \phi) &= 0, \\ \left(\frac{\partial w}{\partial t}, \phi\right) + a_w(w; u, \phi) &= f(u, \phi), \end{aligned}\right\} \tag{3.1}$$

for all $\phi \in H^1(\Omega)$, where

$$\begin{aligned} a_u(u; u; v, \phi) &= d_1 \int_\Omega \nabla u \cdot \nabla \phi \, dx - \chi \int_\Omega u \nabla v \cdot \nabla \phi \, dx - \lambda \int_\Omega u(1 - u - v)\phi \, dx, \\ a_v(v; v; u; w, \phi) &= \eta \int_\Omega v w \phi \, dx - \rho \int_\Omega v(1 - u - v)\phi \, dx, \\ a_w(w; u, \phi) &= d_2 \int_\Omega \nabla w \cdot \nabla \phi \, dx + \int_\Omega w(\alpha u + \beta)\phi \, dx, \\ f(u, \phi) &= \int_\Omega \alpha u \phi \, dx. \end{aligned}$$

Note that $u \in L^2(0, I, H^1(\Omega))$ and $u' \in L^2(0, I, H^{-1}(\Omega))$ imply that $t \mapsto u(t)$ as a mapping from $[0, I]$ in $L^2(\Omega)$ is continuous. Here $H^{-1}(\Omega)$ is the dual space of $H^1(\Omega)$.

3.2. Discrete problem

In this section, we first present the temporal discretization of the coupled variational system (3.1). In particular, the application of Crank–Nicolson time discretization is discussed for the system.

3.2.1. Temporal discretization

Let $0 = t^0 < t^1 < \cdots < t^N = I$ be a decomposition of the considered time interval $[0, I]$, and $\delta_t = t^{n+1} - t^n$, $n = 0, 1, \ldots, N-1$ denotes the uniform time step. Also, we use $u^n(x) := u(x, t^n)$, $v^n(x) := v(x, t^n)$, $w^n(x) := w(x, t^n)$ to denote the approximation of the solutions at time t^n. After applying the implicit Crank–Nicolson discretization scheme, which is second order and A-stable, the semi-discrete (continuous in space) form of the system (3.1) reads:

For given u^{n-1}, v^{n-1} and w^{n-1} with $u^0 = u_0$, $v^0 = v_0$ and $w^0 = w_0$, find u^n, v^n, $w^n \in H^1(\Omega)$ such that

$$\left.\begin{aligned} \left(\frac{u^n - u^{n-1}}{\delta_t}, \phi\right) + \frac{1}{2}a_u(u^n; u^n; v^n, \phi) &= -\frac{1}{2}a_u(u^{n-1}; u^{n-1}; v^{n-1}, \phi), \\ \left(\frac{v^n - v^{n-1}}{\delta_t}, \phi\right) + \frac{1}{2}a_v(v^n; v^n; u^n; w^n, \phi) &= -\frac{1}{2}a_v(v^{n-1}; v^{n-1}; u^{n-1}; w^{n-1}, \phi), \\ \left(\frac{w^n - w^{n-1}}{\delta_t}, \phi\right) + \frac{1}{2}a_w(w^n; u^n, \phi) &= -\frac{1}{2}a_w(w^{n-1}; u^{n-1}, \phi) + f\left(\frac{u^n + u^{n-1}}{2}, \phi\right), \end{aligned}\right\} \tag{3.2}$$

for all $\phi \in H^1(\Omega)$.

3.2.2. Solution of the nonlinear system

In addition to the nonlinearity in the semi-discrete form of the system (3.2), the coupling between the equations makes the computations more challenging. A fully implicit treatment of the nonlinear and coupled terms leads to a coupled, nonlinear algebraic system, and it will be very challenging to solve this system with a nonlinear solver. Contrarily, an explicit treatment of the nonlinear and the coupled terms leads to a linearized system in which the equations can be solved simultaneously. However, it may impose a severe restriction on the time step. Therefore, we propose an iteration of fixed point type [68] to treat the nonlinear and coupled terms semi-implicitly.

Let us briefly explain the fixed point iteration steps for a nonlinear term in the cancer density equation in the time interval (t^{n-1}, t^n). Let $u_0^n = u^{n-1}$ and the nonlinear integral terms in the cancer density equation are replaced with

$$\begin{aligned} \int_\Omega u_k^n \nabla v_k^n \cdot \nabla \phi \, dx &\simeq \int_\Omega u_k^n \nabla v_{k-1}^n \cdot \nabla \phi \, dx, \\ \int_\Omega u_k^n (1 - u_k^n - v_k^n)\phi \, dx &\simeq \int_\Omega u_k^n (1 - u_{k-1}^n - v_{k-1}^n)\phi \, dx \end{aligned}$$

for $k = 0, 1, 2, \ldots$. We iterate until the residual of the system (3.2) is less than the prescribed threshold value (10^{-8}) or until the given maximal number of iteration is reached. Finally, we set, $u^n = u_k^n$ and advance to the next time step. Using the above prescribed iteration of fixed point type, the nonlinear and coupled terms in all other equations are also handled in a similar way. Thus the linearized (semi-implicit) form of the semi-discrete system (3.2) in the interval (t^{n-1}, t^n) reads:

For given $u_0^n = u^{n-1}$, $v_0^n = v^{n-1}$ and $w_0^n = w^{n-1}$ with $u^0 = u(x, 0)$, $v^0 = v(x, 0)$ and $w^0 = w(x, 0)$, find u_k^n, v_k^n and w_k^n such that for all $\phi \in H^1(\Omega)$

$$\left.\begin{aligned} \left(u_k^n, \phi\right) + \frac{\delta_t}{2} a_u\left(u_k^n; u_{k-1}^n; v_{k-1}^n, \phi\right) &= \left(u^{n-1}, \phi\right) - \frac{\delta_t}{2} a_u\left(u^{n-1}; u^{n-1}; v^{n-1}, \phi\right), \\ \left(w_k^n, \phi\right) + \frac{\delta_t}{2} a_w\left(w_k^n; u_k^n, \phi\right) &= \delta_t f\left(\frac{u_k^n + u^{n-1}}{2}, \phi\right) + \left(w^{n-1}, \phi\right) - \frac{\delta_t}{2} a_w\left(w^{n-1}; u^{n-1}, \phi\right), \\ \left(v_k^n, \phi\right) + \frac{\delta_t}{2} a_v\left(v_k^n; v_{k-1}^n; u_k^n; w_k^n, \phi\right) &= \left(v^{n-1}, \phi\right) - \frac{\delta_t}{2} a_v\left(v^{n-1}; v^{n-1}; u^{n-1}; w^{n-1}, \phi\right), \end{aligned}\right\} \tag{3.3}$$

for $k = 0, 1, 2, \ldots$.

The system (3.3) satisfies the residual condition within two or three iteration steps for the considered parameters and time step, thus the application of the fixed point iteration is sufficient. Nevertheless, the number of iterations will increase when the time step δ_t is increased.

3.2.3. Finite element discretization

Let Ω_h be a triangulation of Ω into triangles. Suppose $V_h \subset H^1(\Omega)$ is a conforming finite element (finite dimensional) subspace of $H^1(\Omega)$ with basis functions $\phi_h := \phi_i, i = 1, 2, \ldots, \mathcal{N}$ such that $V_h := \text{span}\{\phi_i\}$, where $\mathcal{N}$ is the number of degrees of freedom (solutions points). Further, define the finite element ansatz functions and its gradient as

$$u_h^n(x) = \sum_{i=1}^{\mathcal{N}} u_i^n \phi_i(x), \qquad v_h^n(x) = \sum_{i=1}^{\mathcal{N}} v_i^n \phi_i(x), \qquad w_h^n(x) = \sum_{i=1}^{\mathcal{N}} w_i^n \phi_i(x),$$

$$\nabla u_h^n(x) = \sum_{i=1}^{\mathcal{N}} u_i^n \nabla\phi_i(x), \qquad \nabla v_h^n(x) = \sum_{i=1}^{\mathcal{N}} v_i^n \nabla\phi_i(x), \qquad \nabla w_h^n(x) = \sum_{i=1}^{\mathcal{N}} w_i^n \nabla\phi_i(x),$$

where u_i^n, v_i^n and w_i^n are the unknown solution coefficients. Using the discrete form of the functions in (3.3) and testing for each basis functions lead to a set of linearized (semi-implicit) system of algebraic equations

$$\left.\begin{aligned} \left(M + \frac{\delta_t}{2} A^u\right) \mathcal{U}^n &= \left(M - \frac{\delta_t}{2} \tilde{A^u}\right) \mathcal{U}^{n-1}, \\ \left(M + \frac{\delta_t}{2} A^w\right) \mathcal{W}^n &= \left(M - \frac{\delta_t}{2} \tilde{A^w}\right) \mathcal{W}^{n-1} + \delta_t \left(F + \tilde{F}\right), \\ \left(M + \frac{\delta_t}{2} A^v\right) \mathcal{V}^n &= \left(M - \frac{\delta_t}{2} \tilde{A^v}\right) \mathcal{V}^{n-1}, \end{aligned}\right\} \tag{3.4}$$

where $\mathcal{U}^n = \text{vec}(\mathcal{U}^n)$, $\mathcal{V}^n = \text{vec}(\mathcal{V}^n)$ and $\mathcal{W}^n = \text{vec}(\mathcal{W}^n)$ are the vectorization of the solution matrices $\mathcal{U}^n = [u_j^n]$, $\mathcal{V}^n = [v_j^n]$, and $\mathcal{W}^n = [w_j^n]$, respectively. Further, denote the fully discrete solutions by $u_{h,k}^n$, $v_{h,k}^n$ and $w_{h,k}^n$ at a fixed point step $k = 0, 1, 2, \ldots$. Moreover, the entries of the mass, stiffness matrices and source vector at a fixed point iteration step k are given by

$$\begin{aligned} M_{ij} &= \int_{\Omega_h} \phi_i(x)\, \phi_j(x)\, dx, \\ A_{ij}^u &= d_1 \int_{\Omega_h} \nabla\phi_i(x) \cdot \nabla\phi_j(x)\, dx - \chi \int_{\Omega_h} \phi_i(x)\, \nabla v_{h,k-1}^n \cdot \nabla\phi_j(x)\, dx \\ &\quad - \lambda \int_{\Omega_h} \phi_i(x)\, (1 - u_{h,k-1}^n - v_{h,k-1}^n)\, \phi_j(x)\, dx, \\ \tilde{A^u}_{ij} &= d_1 \int_{\Omega_h} \nabla\phi_i(x) \cdot \nabla\phi_j(x)\, dx - \chi \int_{\Omega_h} \phi_i(x)\, \nabla v_h^{n-1} \cdot \nabla\phi_j(x)\, dx \\ &\quad - \lambda \int_{\Omega_h} \phi_i(x)\, (1 - u_h^{n-1} - v_h^{n-1})\, \phi_j(x)\, dx, \\ A_{ij}^w &= d_2 \int_{\Omega_h} \nabla\phi_i(x) \cdot \nabla\phi_j(x)\, dx + \int_{\Omega_h} \phi_i(x)\, (\alpha u_{h,k}^n + \beta)\, \phi_j(x)\, dx, \end{aligned}$$

$$\tilde{A^w}_{ij} = d_2 \int_{\Omega_h} \nabla\phi_i(x) \cdot \nabla\phi_j(x)\, dx + \int_{\Omega_h} \phi_i(x)\ (\alpha u_h^{n-1} + \beta)\ \phi_j(x)\, dx,$$

$$F_i = \alpha \int_{\Omega_h} u_{h,k}^n\, \phi_i(x)\, dx$$

$$\tilde{F}_i = \alpha \int_{\Omega_h} u_h^{n-1}\, \phi_i(x)\, dx$$

$$A_{ij}^v = \eta \int_{\Omega_h} \phi_i(x)\ w_{h,k}^n\, \phi_j(x)\, dx - \rho \int_{\Omega_h} \phi_i(x)\ (1 - u_{h,k}^n - v_{h,k-1}^n)\, \phi_j(x)\, dx,$$

$$\tilde{A^v}_{ij} = \eta \int_{\Omega_h} \phi_i(x)\ w_h^{n-1}\, \phi_j(x)\, dx - \rho \int_{\Omega_h} \phi_i(x)\ (1 - u_h^{n-1} - v_h^{n-1})\, \phi_j(x)\, dx.$$

4. Numerical experiments

First, we perform a convergence study for the proposed numerical scheme with known analytical solutions, and then a mesh convergence study with the cancer model parameters. After that proposed finite element scheme will be validated using existing numerical results in the literature for the coupled nonlinear cancer invasion model. Further, throughout the subsequent sections initial cancer density and ECM density and MDE concentration are assumed as in Section 2.2. Finally, an array of computations are performed to study the effects of the proliferation rate, haptotactic coefficient and ECM remodelling rate on the cancer invasion.

The computations are performed on the unit square domain $\Omega = [0, 1] \times [0, 1]$, discretized uniformly using triangular elements with mesh size $h = 0.0220971$. Further, piecewise linear finite elements for all unknown variables and a time step $\delta_t = 0.001$ in the Crank–Nicolson scheme are used. The numerical scheme is implemented in our in-house finite element package [62], and the system of algebraic equations is solved using UMFPACK [69,70]. Computations are performed using Intel(R) Core(TM) i7-3770s CPU with 3.10 GHZ and 8 GB RAM.

4.1. Convergence study with known analytic solution

In this section, we consider the coupled model (2.2) with source terms,

$$\left.\begin{aligned} \frac{\partial u}{\partial t} - d_1\Delta u + \nabla\cdot(\chi u\nabla v) - \lambda u(1-u-v) &= f_u,\\ \frac{\partial v}{\partial t} + \eta v w - \rho v(1-u-v) &= f_v,\\ \frac{\partial w}{\partial t} - d_2\Delta w - \alpha u(1-w) + \beta w &= f_w. \end{aligned}\right\} \tag{4.1}$$

The source terms f_u, f_v and f_w are chosen so that the system (4.1) satisfies the analytical solution

$$u = e^t \sin(2\pi x)\sin(2\pi y), \qquad v = e^{-t}\sin(2\pi x)\sin(2\pi y), \qquad w = e^t \sin(2\pi x)\sin(2\pi y),$$

with the dimensionless parameters

$$d_1 = 0.001, \qquad d_2 = 0.008, \qquad \lambda = 0.75, \qquad \chi = 0.005, \qquad \eta = 5, \qquad \rho = 1, \qquad \alpha = 0.25, \qquad \beta = 0.5.$$

A set of finite element computations on uniformly refined meshes with $\delta_t = h$ are performed. The coarsest triangular mesh level contains 25 degrees of freedom (DOF) for each unknown u, v, and w with the mesh size $h = 0.353553$, and a sequence of fine mesh levels are obtained by refining the coarsest mesh uniformly. It results in 4225 DOF for each unknown function with $h = 0.0220971$ on the finer mesh.

Furthermore, to compare the discretization errors at different mesh levels and to verify the order of convergence of the numerical scheme, the following errors are computed

$$E_1 := L^2\left(0, I; L^2(\Omega)\right) = \int_0^I \left(\|u(t) - u_h(t)\|^2_{L^2(\Omega)}\right) dt,$$

$$E_2 := l^\infty\left(0, I; L^2(\Omega)\right) = \sup_{n=1,\ldots,N} \|u(t^n) - u_h(t^n)\|_{L^2(\Omega)}.$$

The obtained numerical errors are depicted in Fig. 2. As expected, Fig. 2(i) shows a second order convergence of the error with L^2-norm in space and time. Similarly, Fig. 2(ii) also shows a second order convergence of the error with L^∞ norm in time and L^2-norm in space. These plots confirm that the optimal order of convergence (approximately two) for both cases with the piecewise linear triangular (P_1) finite elements is acquired.

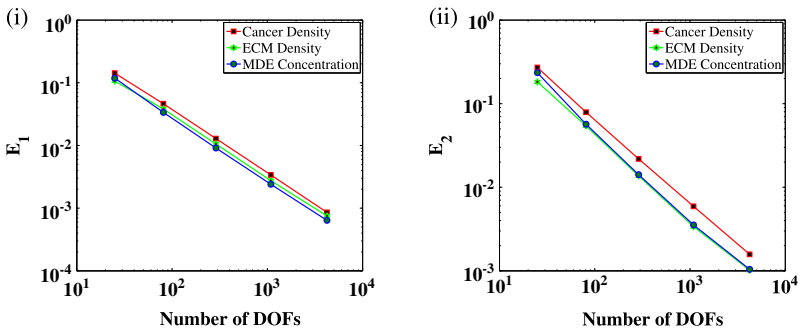

Fig. 2. Error plots of the cancer cell density, ECM density and MDE concentration obtained with different mesh levels for the scheme convergence study. Panel (i) and (ii), respectively represent the logarithmic values of E_1 and E_2 errors of the solution of the system (2.2) against the logarithmic value of the DOF.

4.2. Mesh independent test for cancer model

Mesh convergence study is one of the standard numerical tests used to obtain a mesh independent solution. Further, it evaluates the robustness of a numerical scheme. In order to perform the mesh convergence study for the proposed finite element scheme, the following dimensionless parameters are used:

$$d_1 = 0.0001, \quad d_2 = 0.0005, \quad \lambda = 0.75, \quad \chi = 0.005, \quad \eta = 10, \quad \rho = 1.5,$$
$$\alpha = 0.25, \quad \beta = 0.5.$$

Moreover, the initial mesh level (L0) consists of 1089 degrees of freedom (unknown solution coefficients) for each unknown variable with the mesh size $h = 0.0441942$. The successive mesh levels (L1 and L2) are obtained by refining the initial mesh uniformly.

The mesh convergence results are depicted in Fig. 3 and to better visualize their behaviour, the cancer cells density, ECM density and MDE concentration are plotted along the line $y = x$, that is, along the arc length from origin $r = \sqrt{2}x$ in Ω. Moreover, the solutions need not be radially symmetric due to the choice of diffusion and haptotaxis coefficients in the model equations, and therefore the behaviours of the solution need not be same for all lines over the domain.

The first row in Fig. 3 represents the cancer cell density obtained with L0, L1 and L2 meshes at different times $t = 10$ and $t = 20$, whereas the second and third rows of Fig. 3 show the ECM density and the MDE concentration respectively. The evolution of the cancer cell and its interaction with ECM by producing MDE can clearly be seen in Fig. 3. Cancer cells grow according to $\lambda = 0.75$, while haptotaxis accelerates the invasion of cancer cells into the ECM. The process of invasion is clearly visible in Fig. 3, for instance, the cancer cells invaded nearly half away of the ECM domain at $t = 20$. It is achieved through the production of more MDE by the cancer cells, see the third row of Fig. 3.

Even though the difference between the solutions obtained with L0, L1 and L2 meshes is very small, a close look at these plots clearly show the mesh convergence behaviour. The solutions obtained with L1 and L2 meshes are almost identical, and it shows that a mesh with $h = 0.0220971$ is sufficient for a mesh independent solution. Therefore, the L1 mesh is used in all our further computations, and it results in 4225 degrees of freedom for each equation, that is, 12,675 degrees of freedom all together for the system.

4.3. Validation

To validate the proposed finite element scheme for the cancer model, we compare the computed solution with the numerical results published in [32]. In the validation test example, we use the same dimensionless values used in [32], that is,

$$d_1 = 0.0001, \quad d_2 = 0.0005, \quad \lambda = 0.75, \quad \chi = 0.00005, \quad \eta = 10, \quad \rho = 0.0,$$
$$\alpha = 0.1, \quad \beta = 0.$$

A finite element computation is performed in the unit square domain with $L1$ mesh. However, in order to compare the finite element solution with the numerical results in [32], the cancer cell density, ECM density and MDE concentration are plotted only along the line $y = 0$, that is along the arc length from origin $r = x$ in Fig. 4. The continuous lines denote the finite element solutions, whereas the dotted lines are the solutions reported in [32]. The finite element solutions, the density of cancer cells, ECM density and concentration of MDE agree well with the solutions reported in [32].

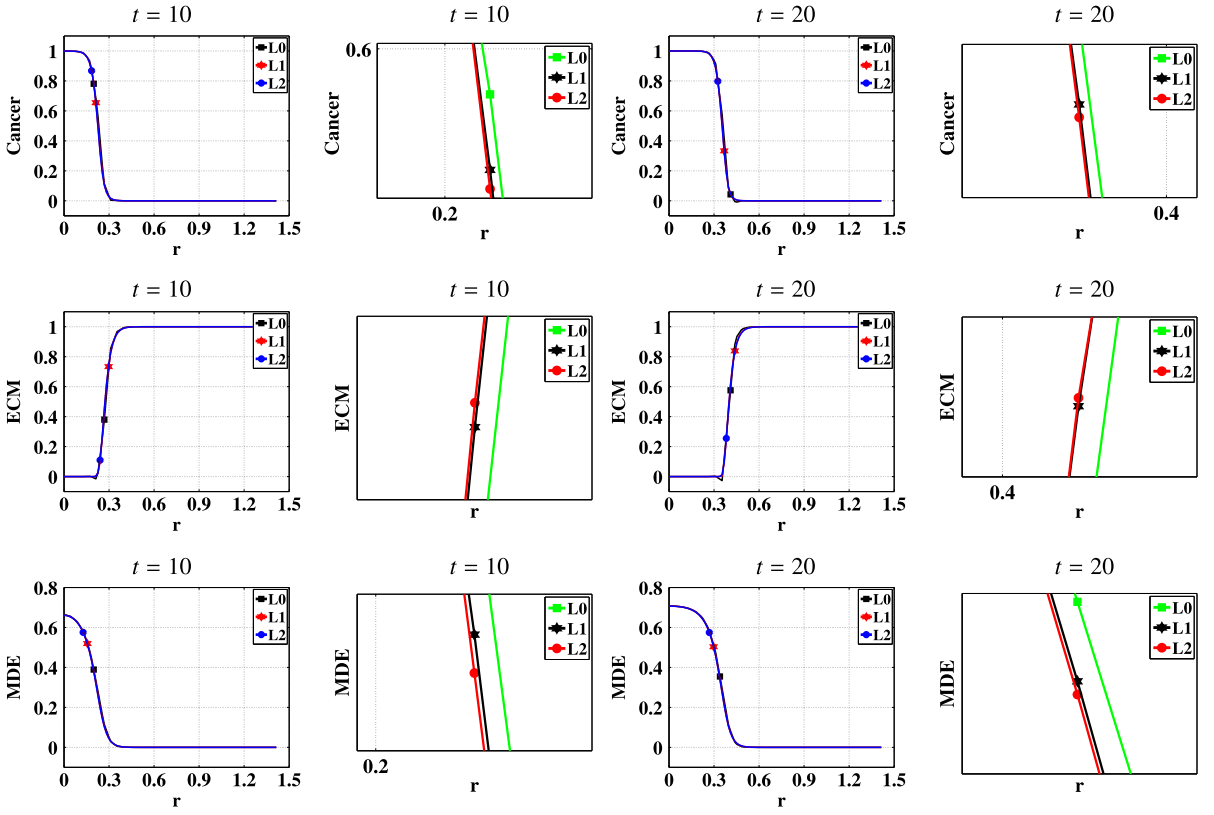

Fig. 3. Evolution of the cancer cell density, ECM density and MDE concentration along the line $y = x$ at different times, $t = 10, 20$, obtained with different mesh levels. The second and fourth columns are the magnification of the first and third columns, respectively.

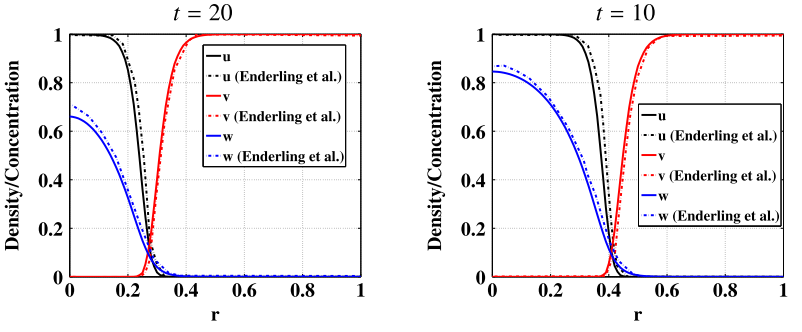

Fig. 4. Comparison of the finite element solutions along the line $y = 0$, with the results presented in Enderling et al. [32].

4.4. Effects of haptotactic coefficient

We first study the influence of the haptotactic coefficient on the cancer invasion dynamics by varying χ. In this study, we consider three variants of haptotactic coefficient: (i) $\chi = 0.05$, (ii) $\chi = 0.15$ and (iii) $\chi = 0.25$ with a small proliferation rate of cancer cells, that is, $\lambda = 0.01$. Further, it is assumed that there is no remodelling effect of ECM, that is, $\rho = 0$. Moreover, we used $\alpha = 0.50$ and $\beta = 0.4$, whereas all other parameters are chosen as in the previous validation example in Section 4.3. All computations have been performed imposing $I = 30$ and time step $\delta_t = 0.001$. Further we triangulate the domain uniformly with maximum mesh size $h = 0.0220971$.

The obtained numerical results of the cancer cells density ((i), (iii), (v)) and the ECM density ((ii), (iv), (vi)) at different instances, $t = 5, 10, 15, 20$ are depicted in Fig. 5 for all three variants, showing the effects of haptotactic coefficient. In the first test case, $\chi = 0.05$, the snapshot at $t = 5$, shows that the cancer density reduces at the origin, and starts migrating towards the direction of the gradient of ECM: this last eventually degrades by increasing MDE production, see the first snapshot in the second row of Fig. 5. A similar behaviour is observed at $t = 10$, where the migration of the cancer cells becomes more clear. Moreover, the haptotaxis effect can clearly be seen at $t = 15$ and $t = 20$, where the small cluster of

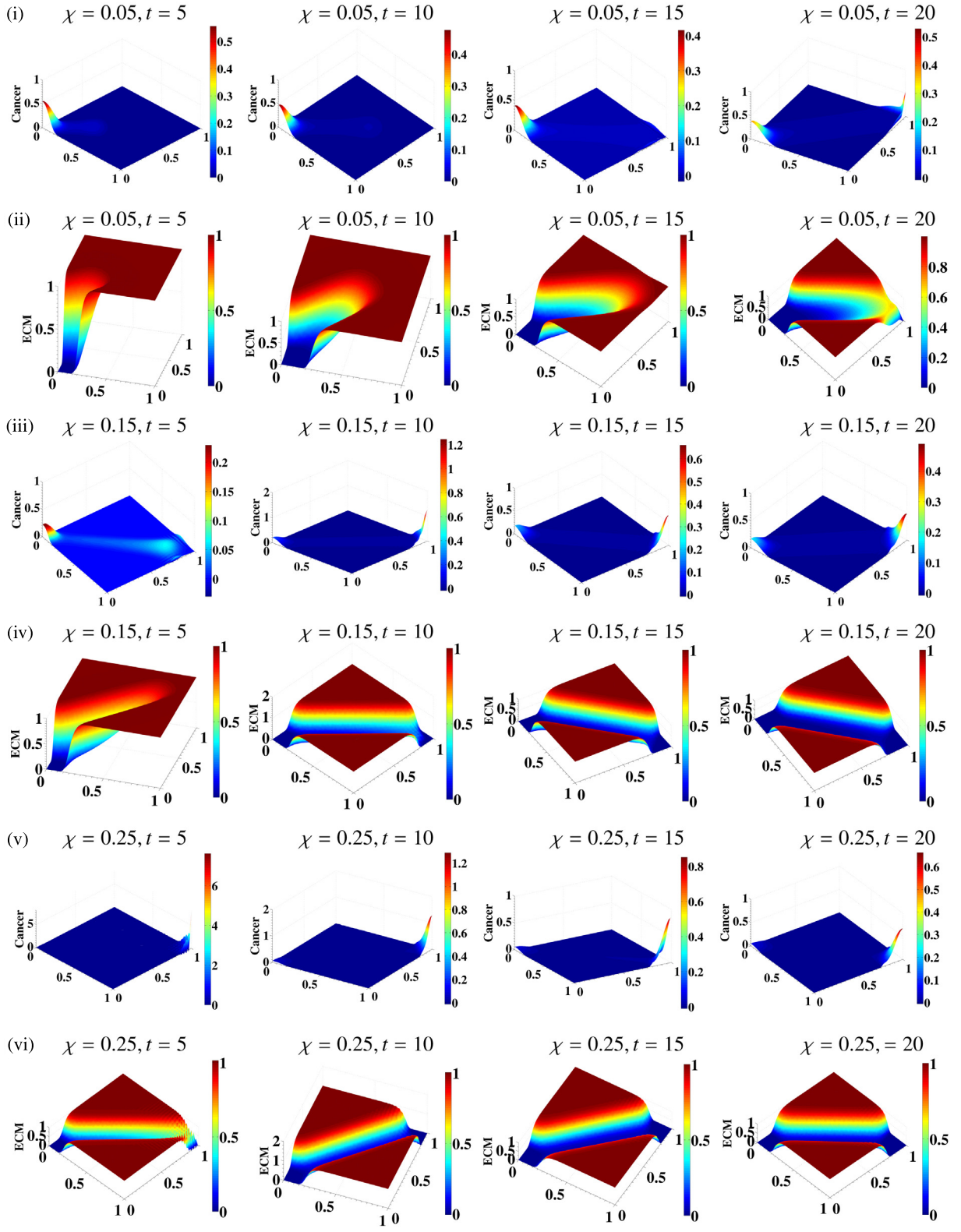

Fig. 5. Sequence of images showing the effects of haptotactic coefficients on cancer cell density ((i), (iii), (v)) and ECM density ((ii), (iv), (vi)) at different times $t = 5$, 10, 15, 20 and haptotaxis coefficient values of $\chi = 0.05, 0.15, 0.25$. All other parameters of the model (2.2) are fixed as in Section 4.4.

cancer cells becomes larger at this stage. Further, the cancer cells migrate along the direction of the ECM gradient and reach the boundary of the domain, see the last snapshot in the first and second rows of Fig. 5.

Haptotaxis effect increases when the haptotactic coefficient rapidly increases, see the cancer cells and ECM snapshots for $\chi = 0.15$ and $\chi = 0.25$ in Fig. 5. An increase in χ value accelerates the cancer cells migration, and degrades the ECM by MDE rapidly even at low proliferation rate of cancer cells. Also, the cancer cells reach the boundary of the domain quickly, at $t = 10$ for $\chi = 0.15$ and at $t = 5$ for $\chi = 0.25$, due to the acceleration induced by the large value of χ. Moreover, the density of cancer cells increases near to the boundary of the domain when $\chi = 0.15, 0.25$ at dimensionless time 10 and 15.

4.5. Effects of cancer cell proliferation rate

Here, next we have shown the influence of the cancer cell proliferation coefficient on the cancer invasion model, for, $\lambda = 0.0, 0.25, 0.5, 0.75, 1.0, 1.5$. In all these simulations, we used $\chi = 0.005$, $\eta = 10$, $\rho = 0.5$, $\alpha = 0.5$, and $\beta = 0.4$, whereas d_1, d_2, and δ_t are chosen as in Sections 4.2 and 4.3.

Snapshots of the cancer cell density obtained with different proliferation rates, $\lambda = 0.0, 0.5, 1.5$, for $t = 5, 10, 20, 30$, are depicted in Fig. 6((i)–(iii)). Further, the cancer cell density, ECM density and MDE concentration along the line $y = x$ are also plotted in Fig. 6((iv)-(vi)). Here, initial in last three panel rows, ((iv)–(vi)), of Fig. 6 represents the imposed initial conditions as in Section 2.2. It should be noted that an increase in the growth rate of tumours, due to malignant mutations as well changes in the tumour micro-environment, cause an accelerated invasion of cancer cells into the ECM domain.

Let us now consider the variant $\lambda = 0.0$, that is, no growth in the cancer cell density. In this variant, there is no malignant effect in the cancer invasion during the initial stage, at time $t = 5$, see first plot of Fig. 6(i). Further, cancer cell density and MDE concentration decrease from initial level due to diffusion and $\lambda = 0.0$ value, even though a small cluster of cancer cells is formed over the initial period, which migrates nearly half of the ECM domain. Similar effects also appeared at different times, $t = 10, 20, 30$, see Fig. 6.

Now, let us consider the variant $\lambda = 0.5$. Though the density of the cancer cell slightly decreases from the initial value, the reduction is not as in the variant $\lambda = 0.0$, and the malignant effect starts at $t = 10$. However, over the period, from $t = 10$ to $t = 30$, the cancer invasion increases, and it can clearly be seen from the snapshots in the second row of Fig. 6. Eventually, the cancer cells degrade more than half of the ECM domain.

Finally, the malignant effect is observed at the initial stage itself, on $t = 5$ in the variant $\lambda = 1.5$, as expected, due to the high proliferation rate, see first plot of Fig. 6(iii). Cancer cells produce more degrading enzymes with a higher proliferation rate, see the last row of Fig. 6. Eventually, the higher concentration of MDE degrades more region of ECM. It helps the cancer cells to invade the ECM domain rapidly through the haptotactic effect. Further, the density of the cancer cells attains the threshold value in more than half of the ECM domain, see the third row of Fig. 6 at $t = 20$ and $t = 30$. In particular, cancer cells complete invasion in three-quarters of the ECM region at $t = 30$, when $\lambda = 1.5$ is used.

We finally undertake some computational experiments for different values of proliferation rate and comparison plots are given in the last three rows of Fig. 6 respectively to establish the interactions of cancer density, ECM density and MDE concentration where the numerical experiments are carried out for different time steps namely at $t = 5$, 10, 20 and 30. As expected, increasing the λ value, both MDE production and ECM degradation increase, as well the invasion speed of cancer cells, for all the considered time intervals, see Fig. 6((iv)–(vi)), resulting in a growing degree of malignancy.

4.6. Effects of ECM remodelling rate

Finally, we study the influence of remodelling rate of ECM density on the cancer invasion model. In this study, we consider the following variants of the ECM remodelling rate: (i) $\rho = 0$, (ii) $\rho = 1$, (iii) $\rho = 1.5$, (iv) $\rho = 2.5$ and (v) $\rho = 3.5$ with the cancer cell proliferation rate $\lambda = 0.5$. Moreover, all other parameters of the dimensionless cancer invasion model (2.2) are chosen as in Section 4.5.

The results obtained for $t = 5$, 10, 20, 30, along the line $y = x$ are presented in Fig. 7. Further, initial in the panel rows of Fig. 7 represents the imposed initial conditions of ECM as in Section 2.2. Over the period, the cancer cells continue to migrate to the ECM. In the variant $\rho = 0$, the invasion process is dominant over the ECM remodelling rate, and thus the cancer cells invaded almost half of the ECM domain. An increase in the ECM remodelling rate slows down the invasion process, for instance, the cancer invaded area in the variant $\rho = 1$ is less than the invaded area in the variant $\rho = 0$. This effect can clearly be seen in the variant $\rho = 3.5$, where the cancer invaded area is comparatively small among all other considered variants.

5. Summary

A mathematical model that describes the invasion of cancer cells into the ECM domain by producing MDE is considered. A finite element scheme using the Galerkin finite element method is proposed for computations of the cancer invasion model to study the interactions of cancer cells with the ECM and the degradation of the ECM by MDE. The nonlinear terms in the coupled equations are treated semi-implicitly using an iteration of fixed point type, and therefore a nonlinear solver such as Newtons solver is not necessary. In addition to the convergence with analytical solution and the mesh convergence

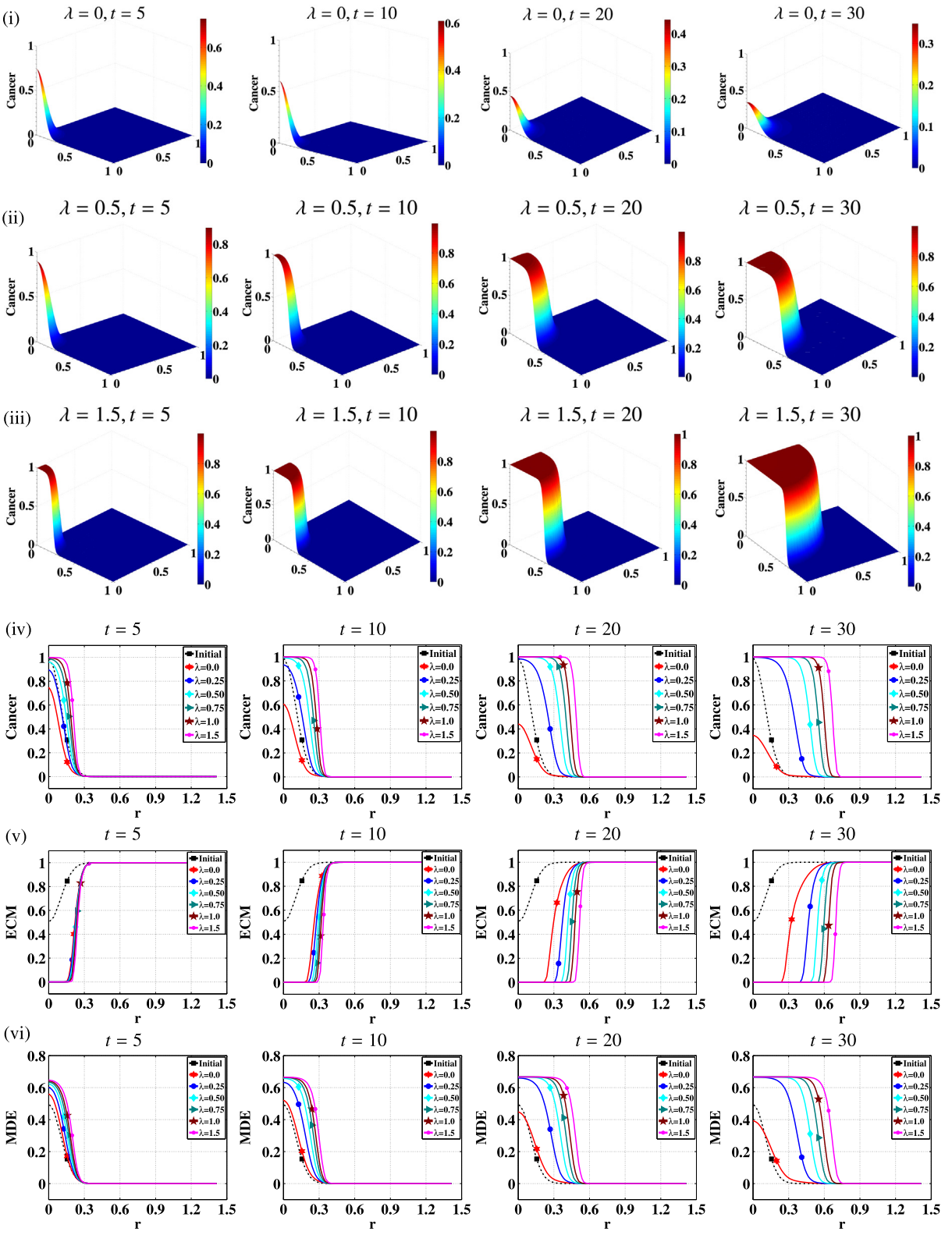

Fig. 6. Sequence of images in first three rows ((i)–(iii)) shows the evolution of cancer density at different times $t = 5, 10, 20$, for different cancer cell proliferation rates $\lambda = 0, 0.5, 1.5$. All other parameters of the model (2.2) are fixed as in Section 4.5. The effects of cancer cell proliferation rate on the cancer density, ECM density and MDE concentration along the line $y = x$ at different times and different proliferation values are shown in the last three rows ((iv)–(vi)).

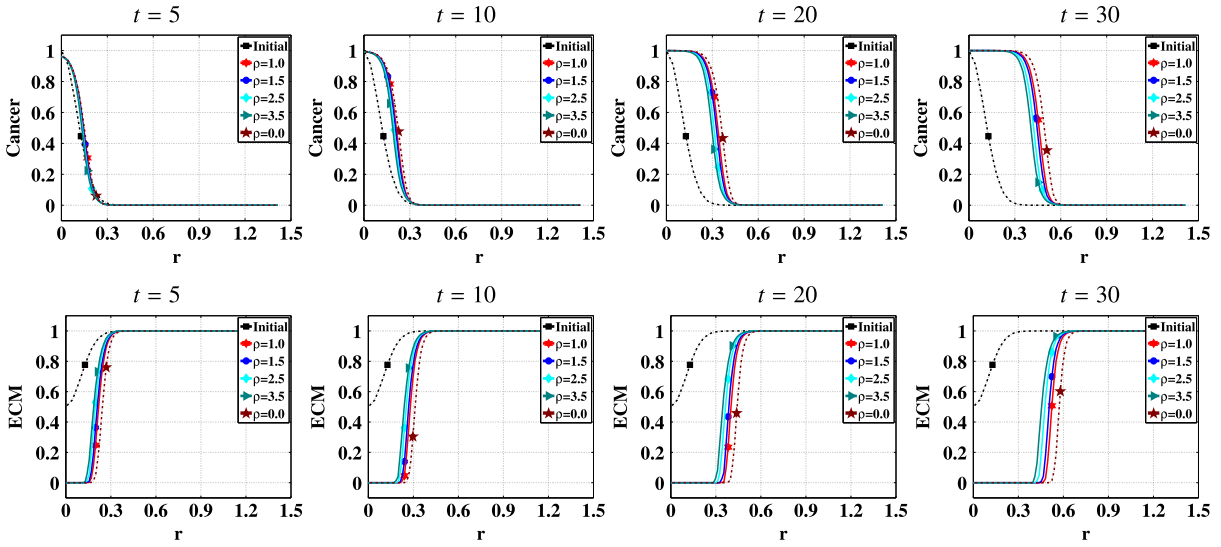

Fig. 7. Effects of ECM remodelling rate on u and v along the line $y = x$. All other parameters are fixed as in Section 4.6.

study, the numerical scheme is validated using existing results in the literature. A number of computations are performed to understand the spatio-temporal behaviours of the cancer invasion process for different values of cancer proliferation rate, haptotactic coefficient and remodelling rate of the ECM.

We have observed that an increase in the haptotactic rate increases the formation of cancer cells and their invasion into the ECM domain rapidly, also helping them to break away from the primary tumour to form secondary cancer cells, which migrate towards regions of growing ECM gradient. However, to invade the remaining ECM components, the secondary cancer cells migrate backwards from the boundary of the domain. Since the growth rate of MDE depends on the cancer density, an increase in the cancer cell proliferation rate enhances the cancer density as well as the MDE concentration. Finally, the cancer cells successfully invade the ECM domain even in the case of high values of remodelling rate. Nevertheless, an increase in the remodelling rate of ECM delays the invasion process.

The computations are performed in a two-dimensional domain, the extension of the proposed finite element scheme to three-dimensional domains is straightforward, and in particular to realistic geometries such as breast, brain and other regions. It is the topic of our next paper. Further, stabilization method such as SUPG, LPS for the approximation of solutions with interior and boundary layers in the cancer model will be a subject of our future research work.

Acknowledgements

The authors wish to thank the unanimous referees for their comments and suggestions which improved the quality of the paper. The second author is thankful to the National Board of Higher Mathematics, Department of Atomic Energy (DAE), Mumbai, India for awarding postdoctoral fellowship (Grant No. NBHM/PDF.71/2013/1148) during his stay at Indian Institute of Science, Bangalore and the DST-SERB for awarding Early Career Award (File No. ECR/20l6/000624).

References

[1] A.R.A. Anderson, A hybrid mathematical model of solid tumour invasion: the importance of cell adhesion, Math. Med. Biol. 22 (2005) 163–186.
[2] A.R.A. Anderson, M.A.J. Chaplain, Continuous and discrete mathematical models of tumor-induced angiogenesis, Bull. Math. Biol. 60 (1998) 857–899.
[3] R.P. Araujo, D.L.S. Mcelwain, A history of the study of solid tumour growth:The contribution of mathematical modelling, Bull. Math. Biol. 66 (2004) 1039–1091.
[4] M.A.J. Chaplain, Avascular growth, angiogenesis and vascular growth in solid tumours: The mathematical modelling of the stages of tumour development, Math. Comput. Modelling 23 (1996) 47–87.
[5] M.A.J. Chaplain, The mathematical modelling of tumour angiogenesis and invasion, Acta Biotheor. 43 (1995) 387–402.
[6] M.A.J. Chaplain, G. Lolas, Mathematical modelling of cancer cell invasion of tissue: the role of the urokinase plasminogen activation system, Math. Models Methods Appl. Sci. 15 (2005) 1685–1734.
[7] R.A. Gatenby, E.T. Gawlinski, A reaction–diffusion model of cancer invasion, Cancer Res. 56 (1996) 5745–5753.
[8] B.A. Lloyd, D. Szczerba, M. Rudin, G. Szekely, A computational framework for modeling solid tumour-growth, Phil. Trans. R. Soc. A 366 (2008) 3301–3318.
[9] P. Tracqui, Biophysical models of tumor growth, Rep. Progr. Phys. 72 (2009) 056701.
[10] H. Enderling, M.A.J. Chaplain, Mathematical modeling of tumor growth and treatment, Curr. Pharm. Des. 20 (2014) 4934–4940.
[11] N. Weidner, J.P. Semple, W.R. Welch, J. Folkman, Tumor angiogenesis and metastasis–correlation in invasive breast carcinoma, N. Engl. J. Med. 324 (1991) 1–8.
[12] J. Folkman, Tumor angiogenesis, Adv. Cancer Res. 43 (1985) 175–203.
[13] J. Folkman, Tumor angiogenesis factor, Cancer Res. 34 (1974) 2109–2113.
[14] H. Enderling, Cancer stem cells and tumor dormancy, Adv. Exp. Med. Biol. 734 (2013) 55–71.

[15] L. Holmgren, M.S. O'Reilly, J. Folkman, Dormancy of micrometastases: Balanced proliferation and apoptosis in the presence of angiogenesis suppression, Nature Med. 1 (1995) 149–153.
[16] H. McAneney, S.F.C. ORourk, Investigation of various growth mechanisms of solid tumour growth within the linear-quadratic model for radiotherapy, Phys. Med. Biol. 52 (2007) 1039–1054.
[17] R.K. Sachs, L.R. Hlatky, P. Hahnfeldt, Simple ODE models of tumor growth and anti-angiogenic or radiation treatment, Math. Comput. Modelling 33 (2001) 1297–1305.
[18] J.B. McGillen, E.A. Gaffney, N.K. Martin, P.K. Maini, A general reaction–diffusion model of acidity in cancer invasion, J. Math. Biol. 68 (2014) 1199–1224.
[19] A. Fasano, M.A. Herrero, M.R. Rodrigo, Slow and fast invasion waves in a model of acid-mediated tumour growth, Math. Biosci. 220 (2009) 45–56.
[20] K. Smallbone, D.J. Gavaghan, R.A. Gatenby, P.K. Maini, The role of acidity in solid tumour growth and invasion, J. Theoret. Biol. 235 (2005) 476–484.
[21] C. Markl, G. Meral, C. Surulescu, Mathematical analysis and numerical simulation for a system modelling acid-mediated tumour cell invasion, Int. J. Anal. (2013) (2013) 15. Article ID 878051.
[22] C. Stinner, C. Surulescu, G. Meral, A multiscale model for pH-tactic invasion with time-varying carrying capacities, IMA J. Appl. Math. (2014). http://dx.doi.org/10.1093/imamat/hxu055.
[23] N.K. Martin, E.A. Gaffney, R.A. Gatenby, P.K. Maini, Tumourtromal interactions in acid-mediated invasion: A mathematical model, J. Theoret. Biol. 267 (2010) 461–470.
[24] A.R.A. Anderson, M.A.J. Chaplain, E.L. Newman, R.J.C. Steele, A.M. Thompson, Mathematical modelling of tumor invasion and metastasis, J. Theor. Med. 2 (2000) 129–154.
[25] M.A.J. Chaplain, G. Lolas, Mathematical modelling of cancer cell invasion of tissue: dynamics heterogeneity, Netw. Heterog. Media 1 (2006) 399–439.
[26] N.E. Deakin, M.A.J. Chaplain, Mathematical modeling of cancer invasion: the role of membrane-bound matrix metalloproteinases, Front. Oncol. 70 (2013) 1–9.
[27] A. Gerisch, M.A.J. Chaplain, Mathematical modelling of cancer cell invasion of tissue:Local and non-local models and the effect of adhesion, J. Theoret. Biol. 250 (2008) 684–704.
[28] K.J. Painter, N.J. Armstrong, J.A. Sherratt, The impact of adhesion on cellular invasion processes in cancer and development, J. Theoret. Biol. 264 (2010) 1057–1067.
[29] P. Domschke, D. Trucu, A. Gerisch, M.A.J. Chaplain, Mathematical modelling of cancer invasion: Implications of cell adhesion variability for tumour infiltrative growth patterns, J. Theoret. Biol. 361 (2014) 41–60.
[30] J.R. Branco, J.A. Ferreira, Paula de Oliveira, Mathematical modelling to efficient protocols to control glioma growth, Math. Biosci. 255 (2014) 83–90.
[31] H. Enderling, M.A.J. Chaplain, A.R.A. Anderson, J.S. Vaidya, A mathematical model of breast cancer development, local treatment and recurrence, J. Theoret. Biol. 246 (2007) 245–259.
[32] H. Enderling, A.R.A. Anderson, M.A.J. Chaplain, A.J. Munro, J.S. Vaidya, Mathematical modelling of radiotherapy strategies for early breast cancer, J. Theoret. Biol. 241 (2006) 158–171.
[33] H. Knutsdottir, E. Pálsson, L. Edelstein-Keshet, Mathematical model of macrophage-facilitated breast cancer cells invasion, J. Theoret. Biol. 357 (2014) 184–199.
[34] V. Andasari, A. Gerisch, G. Lolas, A.P. South, M.A.J. Chaplain, Mathematical modelling of cancer cell invaison of tissue: biological insight from mathematical analysis and computational simulations, J. Math. Biol. 63 (2011) 141–171.
[35] I.R. Conde, M.A.J. Chaplain, A.R.A. Anderson, Mathematical modelling of cancer cell invasion of tissue, Math. Comput. Modelling 47 (2008) 533–545.
[36] M.A.J. Chaplain, M. Ganesh, I.G. Graham, Spatio-temporal pattern formation on spherical surfaces: numerical simulation and application to solid tumour growth, J. Math. Biol. 42 (2001) 387–423.
[37] K. Harley, P. van Heijster, R. Marangell, G.J. Pettet, M. Wechselberger, Existence of traveling wave solutions for a model of tumor invasion, SIAM J. Appl. Dyn. Syst. 13 (2014) 366–396.
[38] T. Hillen, K.J. Painter, Convergence of a cancer invasion model to a logistic chemotaxis model, Math. Models Methods Appl. Sci. 23 (2013) 165–198.
[39] A. Matzavinos, M.A.J. Chaplain, Travelling-wave analysis of a model of the immune response to cancer, C. R. Biol. 327 (2004) 995–1008.
[40] G. Meral, C. Surulesu, Mathematical modelling, analysis and numerical simulations for the influence of heat shock proteins on tumour invasion, J. Math. Anal. Appl. 408 (2014) 597–614.
[41] M.A.J. Chaplain, A.M. Stuart, A model mechanism for the chemotactic response of endothelial cells to tumour angiogenesis factor, IMA J. Math. Appl. Med. Biol. 10 (1993) 149–168.
[42] M.A.J. Chaplain, S.R. McDougall, A.R.A. Anderson, Mathematical modeling of tumor-induced angiogenesis, Annu. Rev. Biomed. Eng. 8 (2006) 11.1–11.25.
[43] S.R. McDougall, A.R.A. Anderson, M.A.J. Chaplain, Mathematical modelling of dynamic adaptive tumour-induced angiogenesis: Clinical implications and therapeutic targeting strategies, J. Theoret. Biol. 241 (2006) 564–589.
[44] A. Stephanou, S.R. McDougall, A.R.A. Anderson, M.A.J. Chaplain, Mathematical modelling of the influence of blood rheological properties upon adaptative tumour-induced angiogenesis, Math. Comput. Modelling 44 (2006) 96–123.
[45] M.E. Orme, M.A.J. Chaplain, A mathematical model of vascular tumour growth and invasion, Math. Comput. Modelling 23 (1996) 43–60.
[46] M.E. Orme, M.A.J. Chaplain, Two-dimensional models of tumour angjogenesis and anti-angiogenesis strategies, IMA J. Appl. Math. 14 (1997) 189–205.
[47] A.H. Daarud, K.G. van der Zee, J.T. Oden, Numerical simulation of a thermodynamically consistent four-species tumor growth model, Int. J. Numer. Methods Biomed. Eng. 28 (2012) 3–24.
[48] P. Gerlee, A.R.A. Anderson, An evolutionary hybrid cellular automaton model of solid tumour growth, J. Theoret. Biol. 246 (2007) 583–603.
[49] J.S. Lowengrub, H.B. Frieboes, F. Jin, Y.L. Chuang, X. Li, P. Macklin, S.M. Wise, V. Cristini, Nonlinear modelling of cancer: bridging the gap between cells and tumours, Nonlinearity 23 (2010) R1–R91.
[50] T. Roose, S.J. Chapman, P.K. Maini, Mathematical models of avascular tumor growth, SIAM Rev. 49 (2007) 179–208.
[51] M. Kolev, B. Zubik-Kowal, Numerical solutions for a model of tissue invasion and migration of tumour cells, Comput. Math. Methods Med. (2011) 452320. 16 pages.
[52] A. Chertock, A. Kurganov, A second-order positivity preserving central-upwind scheme for chemotaxis and haptotaxis models, Numer. Math. 111 (2008) 169–205.
[53] N. Kolbe, J. Katuchova, N. Sfakianakis, N. Hellmann, M. Lukacova-Medvidova, Numerical study of cancer cell invasion dynamics using adaptive mesh refinement: the urokinase model, arXiv:1408.0942v1.
[54] R. Strehl, A. Sokolov, D. Kuzmin, D. Horstmann, S. Tureka, A positivity-preserving finite element method for chemotaxis problems in 3D, J. Comput. Appl. Math. 239 (2013) 290–303.
[55] Y. Epshteyn, Discontinuous Galerkin methods for the chemotaxis and haptotaxis models, J. Comput. Appl. Math. 224 (2009) 168–181.
[56] A. Amoddeo, Adaptive grid modelling for cancer cells in the early stage of invasion, Comput. Math. Appl. 69 (2015) 610–619.
[57] A. Amoddeo, Moving mesh partial differential equations modelling to describe oxygen induced effects on avascular tumour growth, Cogent Phys. 2 (2015) 1050080.
[58] A. Amoddeo, Oxygen induced effects on avascular tumour growth: a preliminary simulation using an adaptive grid algorithm, J. Phys.: Conf. Ser. 633 (2015) 012088.
[59] X. Zheng, S.M. Wise, V. Cristini, Nonlinear simulation of tumor necrosis, neo-vascularization and tissue invasion via an adaptive finite-element/level set method, Bull. Math. Biol. 67 (2005) 211–259.
[60] M.E. Hubbard, H.M. Byrne, Multiphase modelling of vascular tumour growth in two spatial dimensions, J. Theoret. Biol. 316 (2013) 70–89.
[61] S. Ganesan, L. Tobiska, Stabilization by local projection for convection–diffusion and incompressible flow problems, J. Sci. Comput. 43 (2010) 326–342.
[62] V. John, G. Matthies, MooNMD - a program package based on mapped finite element methods, Comput. Vis. Sci. 6 (2004) 163–170.
[63] D. Bray, Cell Movements: From Molecules to Motility, Garland Publishing, 2000.
[64] J.A. Sherratt, J.D. Murray, Models of epidermal wound healing, Proc. R. Soc. B 241 (1990) 29–36.

[65] C.L. Stokes, D.A. Lauffenburger, S.K. Williams, Migration of individual microvessel endothelial cells: stochastic model and parameter measurement, J. Cell Sci. 99 (1991) 419–430.
[66] W. Yu, J. Kim, L. Ossowski, Reduction in surface urokinase receptor forces malignant cells into a protracted state of dormancy, J. Cell Biol. 137 (1997) 767–777.
[67] A. Bajpai, J.B. Baker, Cryptic urokinase binding sites on human foreskin fibroblasts, Biochem. Biophys. Res. Commun. 133 (1985) 475–482.
[68] S. Ganesan, L. Tobiska, An accurate finite element scheme with moving meshes for computing 3D-axisymmetric interface flows, Internat. J. Numer. Methods Fluids 57 (2008) 119–138.
[69] T.A. Davis, Algorithm 832: UMFPACK V4.3-an unsymmetric-pattern multifrontal method, ACM Trans. Math. Softw. 30 (2004) 196–199.
[70] T.A. Davis, A column pre-ordering strategy for the unsymmetric-pattern multifrontal method, ACM Trans. Math. Softw. 30 (2004) 167–195.
[71] J. Valenciano, M.A.J. Chaplain, Computing highly accurate solutions of a tumor angiogenesis model, Math. Models Methods Appl. Sci. 13 (2003) 747–766.